



Article

The Optimal Branch Width Convergence Ratio to Maximize the Transport Efficiency of the Combined Electroosmotic and Pressure-Driven Flow within a Fractal Tree-like Convergent Microchannel

Dalei Jing * and Peng Qi

School of Mechanical Engineering, University of Shanghai for Science and Technology, Shanghai 200093, China; qipengjdx@163.com

* Correspondence: jingdalei@usst.edu.cn

Abstract: Building upon the efficient transport capabilities observed in the fractal tree-like convergent structures found in nature, this paper numerically studies the transport process of the combined electroosmotic and pressure-driven flow within a fractal tree-like convergent microchannel (FTCMC) with uniform channel height. The present work finds that the flow rate of the combined flow first increases and then decreases with the increasing branch width convergence ratio under the fixed voltage difference and pressure gradient along the FTCMC, which means that there is an optimal branch width convergence ratio to maximize the transport efficiency of the combined flow within the FTCMC. The value of the optimal branch convergence ratio is highly dependent on the ratio of the voltage difference and pressure gradient to drive the combined flow. By adjusting the structural and dimensional parameters of the FTCMC, the dependencies of the optimal branch convergence ratio of the FTCMC on the branching level convergence ratio, the length ratio, the branching number, and the branching level are also investigated. The findings in the present work can be used for the optimization of FTCMC with high transport efficiency for combined electroosmotic and pressure-driven flow.

Keywords: fractal tree-like structure; branch convergence; electroosmotic flow; pressure-driven flow



Citation: Jing, D.; Qi, P. The Optimal Branch Width Convergence Ratio to Maximize the Transport Efficiency of the Combined Electroosmotic and Pressure-Driven Flow within a Fractal Tree-like Convergent Microchannel. *Fractal Fract.* **2024**, *8*, 279. <https://doi.org/10.3390/fractalfract8050279>

Academic Editor: Alicia Cordero

Received: 18 March 2024

Revised: 1 May 2024

Accepted: 2 May 2024

Published: 7 May 2024



Copyright: © 2024 by the authors. Licensee MDPI, Basel, Switzerland. This article is an open access article distributed under the terms and conditions of the Creative Commons Attribution (CC BY) license (<https://creativecommons.org/licenses/by/4.0/>).

1. Introduction

The continuous development of micro- and nano-fabrication technologies has enabled the vigorous development of microfluidic systems, which could be employed in medical, pharmaceutical, and biological applications due to their advantages such as high efficiency, compactness, and less consumption of chemicals [1,2]. Nevertheless, extremely high fluid resistance has become a major barrier influencing the applications of microfluidic systems because of the tremendously tiny characteristic dimension of the microchannel [3,4], which requires the design of the microchannel layout. In addition, applications in fields such as multiphase reactions, microfluidic sensors, biological analysis, drug delivery, and nanoparticle transportation require precise control of fluid flow in microchannels with a special channel layout [5–7]. Therefore, designing advanced channel configuration in a desirable manner with low fluid resistance or high transport efficiency to deliver liquids or reagents from one point to other points, or vice versa, is usually the core of these applications. Motivated by branching structures in nature with high transport efficiency [8–10], tree-like branched structures have been widely used in the layout design of microfluidics. For example, several scholars introduced the tree-like channel layout into the design of microchannel heat sinks and demonstrated that the tree-like channel layout displayed better hydrothermal performances compared with the traditional serpentine or straight microchannel heat sinks [11–13]. Lab-on-a-chip designed with a tree-like microchannel

arrangement could be used for biomedical detection [14,15]. Introducing the tree-like microchannel into fuel cells [16,17] can not only improve electricity conversion efficiency but also reduce material usage compared with the conventional serpentine channel types, which is crucial for the efficient operation of energy conversion and storage devices.

In contrast to macroscale fluid flow, which could be easily controlled by conventional pressure-driven methods, fluid flow in microfluidic systems might be generated by imposing an electric field or a combination of an electric field and a pressure gradient due to interfacial charge generated at the solid–liquid interface by ionization or adsorption [18–20]. The surface charge results in the redistribution of ions within the liquid, which eventually forms an electric double layer (EDL) near the solid–liquid interfaces consisting of an inner layer known as the Stern layer and an outside diffuse layer. When voltage is applied tangentially to the EDL, an electric body force is imposed on the ions in the diffuse layer of the EDL, generating the electroosmotic flow (EOF) with a plug-like velocity profile [21]. The EOF can not only eliminate the need for mechanical micropumps but is also easy to control and operate, which has been widely used in fields such as lubrication [22], micromixers [23], and micropumps [24]. The transportation efficiencies of EOF alone and when combined with pressure-driven flow (PDF) within microchannels have been extensively researched [25–33]. For example, Dutta et al. [25] established a mathematical model to address the temperature, Nusselt number, and convective heat transfer coefficient of the steady EOF with a random pressure gradient in a two-dimensional parallel microchannel. Babaie et al. [26] investigated the EOF of power-law fluids in the presence of a pressure gradient in a narrow microchannel. Ebrahimi et al. [27] investigated the mixing and heat transfer performances for the combination of EOF and PDF within a T-shaped microchannel. Mondal et al. [28] formulated a theoretical model to address the fluid flow and heat transfer within a rectangular microchannel by considering the combination of EOF and PDF under the conditions of overlapping EDL and high zeta potential. Deng et al. [29] provided the mathematical solutions of steady/unsteady two-layer combined EOF and PDF in a circular microchannel and gave the physical picture of the evolution of a two-layer system towards a steady state. Hegde and Harikrishnan [30] studied the influence of slip on the hydrodynamics of a combined EOF and PDF by applying the power-law fluid model.

For the EOF or the combined EOF and PDF in the tree-like microchannel, Barrot and Colin [34,35] developed analytical models to determine the optimal network architecture for maximizing the flow rate of either EOF alone or the combined EOF and PDF within the tree-like microchannel network. Jing et al. [36,37] numerically analyzed the optimal cross-sectional dimensions ratio of the tree-like microchannel with the highest transport efficiency for the EOF or the combined EOF and PDF under the limitations of thin EDL and low zeta potential.

While much previous research has demonstrated the benefits of the tree-like microchannel on the enhancement of heat and mass transfer performances, the generally employed branches in the literature [9–13,16,17,34–39] are dimensionally homogenous. However, it is worth pointing out that branch convergence is a universal phenomenon for the tree-like branched structures in nature, like human lungs and tree roots. So, the fractal tree-like microchannel composed of convergent branches is more in line with the branching structures in nature. Some existing literature has verified the excellent heat and mass transport efficiency of such tree-like convergent structures compared with the tree-like structures without branch convergence [40–44], making them ideal for applications like the cooling of microelectronic devices and energy storage.

Nevertheless, the transportation process of the combined EOF and PDF within a fractal tree-like microchannel, especially considering the branch convergence, has not been thoroughly addressed. Thus, in contrast to the existing work focusing on the fluid flow within the tree-like microchannel without branch convergence, this paper concentrates on the combined EOF and PDF within a fractal tree-like microchannel consisting of convergent branches and numerically examines the effects of the branch cross-sectional convergence of the fractal tree-like convergent microchannel (FTCMC) on the flow rate of the combined

EOF and PDF. The current study aims to find the optimal branch width convergence ratio of the FTCMC to achieve maximum transport efficiency of the combined EOF and PDF and explores the dependence of the optimal width convergence ratio with various parameters, such as the ratio of voltage difference and pressure difference, level convergence ratio, length ratio, branching number, and branching level of the FTCMC. This work will not only benefit the understanding of the transport process of the combined EOF and PDF within the FTCMC but will also be helpful in the design of a high-efficiency tree-like microfluidic system.

2. Description of the FTCMC

The schematic of a FTCMC with a branching number of 2 and a branching level of 2 is illustrated in Figure 1. To simplify the model, the FTCMC is symmetric with the same branch dimensions at the same branching level. The cross-section shape of the FTCMC is a rectangle with width convergence along the centerline of each branch. The width convergence ratio and height are also uniform across the whole microchannel. In addition, a size constraint of a fixed total channel volume, which is a commonly used size limitation [9,34–37,45,46], is employed. The total channel volume V of the symmetric FTCMC is given as,

$$V = \sum_{i=0}^m V_i N^i = \sum_{i=0}^m S_i H N^i = \frac{1 + \alpha}{2} w_0 l_0 H \frac{1 - (N \alpha \kappa \lambda)^{m+1}}{1 - N \alpha \kappa \lambda} \quad (1)$$

where V_i and S_i are the volume and bottom area of each branch at the i -th branching level, $\alpha = w_{i+1}/w_i$ ($i = 0, 2, 4, \dots$) is the branch convergence ratio of the FTCMC, $\kappa = w_{j+1}/w_j$ ($j = 1, 3, 5, \dots$) is the level convergence ratio, which reflects the convergence of the two subsequent branching levels of the FTCMC, $\lambda = l_{k+1}/l_k$ ($k = 0, 1, 2, \dots$) is the length ratio of the two subsequent branching levels, N is the branching number, m is the branching levels, and H is the channel height.

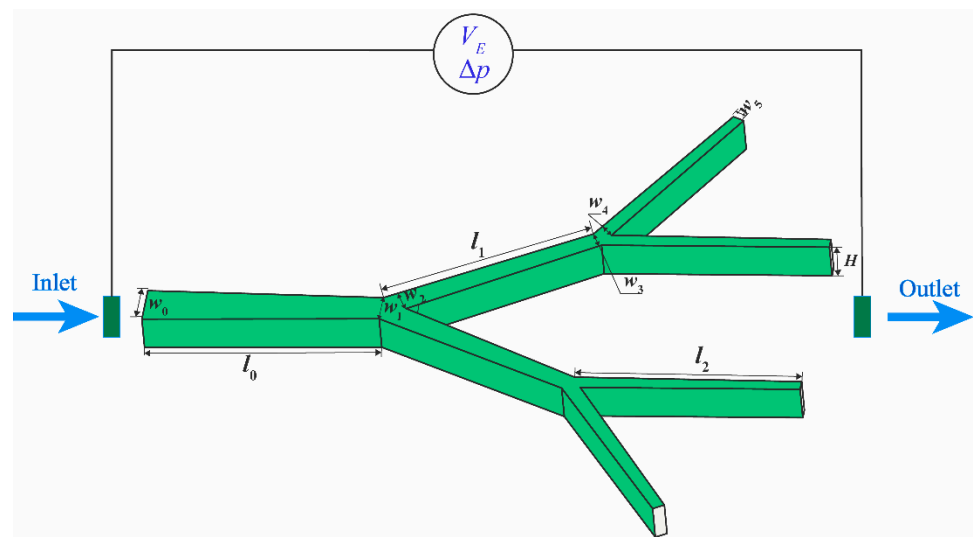


Figure 1. Schematic of FTCMC with $N = 2$ and $m = 2$.

Considering that the dimensions of branch cross-sections, which are highly dependent on the geometric and structural parameters of the FTCMC given in Equation (1), have significant influences on the flow resistance, the present work focuses on the effects of branch widths on the combined PDF and EOF and examines whether an optimal branch

width convergence exists to maximize the flow rate of the combined flow. Under the constraint of the fixed channel volume, the inlet channel width can be given as,

$$w_0 = \frac{2V}{(1 + \alpha)l_0H} \frac{1 - N\alpha\kappa\lambda}{1 - (N\alpha\kappa\lambda)^{m+1}} \tag{2}$$

Subsequently, the widths at two ends of each branch can be given as,

$$\begin{cases} \text{branch inlet : } w_{2i} = \alpha^i \kappa^i w_0 = \frac{2\alpha^i \kappa^i V}{(1+\alpha)^i l_0 H} \frac{1-N\alpha\kappa\lambda}{1-(N\alpha\kappa\lambda)^{m+1}} \\ \text{branch outlet : } w_{2i+1} = \alpha^{i+1} \kappa^i w_0 = \frac{2\alpha^{i+1} \kappa^i V}{(1+\alpha)^i l_0 H} \frac{1-N\alpha\kappa\lambda}{1-(N\alpha\kappa\lambda)^{m+1}} \end{cases} \quad i = 0, 1, 2, \dots \tag{3}$$

Using Equations (2) and (3), we can calculate the branch widths at each branching level when the values of the other parameters are given. The effects of these parameters on the optimal width convergence ratio for maximizing the flow rate of the combined flow within the FTCCM can also be investigated. The values of structural and geometric parameters of FTCCM used in the present work are given in Table 1.

Table 1. Structural and dimensional parameters of FTCCM.

Parameters	Symbol	Value
Branch convergence	α	0.4–1
Level convergence	κ	0.7–1
Length ratio	λ	0.5–1
Branching number	N	2, 3, 4
Branching level	m	0, 1, 2, 3
Channel height	H (μm)	150
Branch angle	β ($^\circ$)	60
Total channel volume	V (μm^3)	3×10^8

3. Numerical Method

3.1. Numerical Setup

To simplify the present problem, the following assumptions are employed:

- (1) The combined EOF and PDF is a three-dimensional incompressible steady and Newtonian fluid flow.
- (2) The channel widths and height of the microchannel are supposed to be much larger than the Debye length to avoid the overlap of EDL.
- (3) Zeta potential at the microchannel wall is uniform and low enough to enable Debye–Hückel linearization.
- (4) No slip condition is applied on the solid–liquid interfaces.

Then, the combined flow can be solved using the following modified Navier–Stokes equation with electrical body force [36,47]:

$$\begin{cases} \nabla v = 0, \\ \rho(v \cdot \nabla v) = -\nabla p + \nabla \cdot (\mu \nabla v) + \rho_e E, \end{cases} \tag{4}$$

where v is the velocity field, ρ is the liquid density, p is the pressure, ρ_e is the net charge density within the EDL, and E is the applied electric field, which is given as follows [36,47]:

$$E = -\nabla \Phi \tag{5}$$

where Φ is the electrical potential of the linear superposition of the applied electric potential φ , and the EDL electric potential ψ is as follows:

$$\Phi = \varphi + \psi \tag{6}$$

According to the electrostatics, the EDL in the microchannel is controlled by the Laplace equation [36,47]:

$$\nabla^2 \varphi = 0 \quad (7)$$

The dependence between the EDL electrical potential ψ in the microchannel and the net charge density ρ_e within the EDL can be described by the coupled Poisson–Boltzmann equation [47,48]:

$$\nabla^2 \psi = -\frac{\rho_e}{\varepsilon_0 \varepsilon_r} = \frac{2n_0 z e}{\varepsilon_0 \varepsilon_r} \sinh\left(\frac{ze\psi}{k_b T}\right) \quad (8)$$

where z is the chemical valence of the liquid, e is the elementary charge, n_0 is the bulk ionic concentration of the liquid, ε_0 is the permittivity of vacuum, ε_r is the relative permittivity of the liquid, k_b is the Boltzmann constant, and T is the absolute temperature of the liquid.

The initial and boundary conditions employed to calculate the combined flow within the FTCCM are summarized as follows:

- (1) Inlet: The voltage V_E is set at the channel inlet, as shown in Equation (9); the pressure P_{in} is maintained at the inlet, as shown in Equation (10); and the inlet ionic concentration is set to 1 mM, as shown in Equation (11),

$$\varphi_{inlet} = V_E \quad (9)$$

$$P_{inlet} = P_{in} \quad (10)$$

$$c_{inlet} = c_0 \quad (11)$$

- (2) Outlet: The outlet potential is set to be zero, as shown in Equation (12); and the outlet pressure is 0 Pa, as shown in Equation (13),

$$\varphi_{outlet} = 0 \quad (12)$$

$$P_{outlet} = 0 \quad (13)$$

- (3) Solid–liquid wall: The Helmholtz–Smoluchowski slip velocity was employed at the solid–liquid wall, and there was no electric potential change given in Equation (14) and no mass flux across the wall given in Equation (15):

$$\mathbf{n} \nabla \varphi = 0 \quad (14)$$

$$\frac{\partial c}{\partial \mathbf{n}} = 0 \quad (15)$$

The values of simulation parameters employed in the present work are listed in Table 2. Applying the above numerical model setup, COMSOL Multiphysics software is used to solve the current problem.

Table 2. Values of simulation parameters.

Parameter	Symbol	Value	Unit
Zeta potential	ζ	−50	mV
Fluid density	ρ	996	kg/m ³
Dynamic viscosity	μ	1×10^{-3}	Pa·s
Relative permittivity	ε_r	80	/
Electric conductivity	σ	5.5×10^{-6}	S/m
Diffusion coefficient	D_c	1×10^{-9}	m ² /s
Bulk ionic concentration	c_0	1	mol/m ³

3.2. Mesh Independence Test and Data Validation

In order to ensure the accuracy of the current numerical study, a computational model with $N = 2$, $m = 2$, $\alpha = 1$, $\kappa = 1$, $\lambda = 1$, and $H = 150 \mu\text{m}$ is used for the mesh independence test. Under the driven voltage of 1000 V and driven pressure of 50 Pa, Table 3 summarizes the data of inlet velocity v_{in} and the outlet volume flow rate Q_v and their relative errors when changing the grid number. The computing time is also given to reflect the computing efficiency. According to the results given in Table 3, the mesh generation with a grid number of 1,350,140 is good enough to obtain numerical results with high accuracy and high computing efficiency, which is subsequently employed for the remaining simulations in this work.

Table 3. Results of the mesh independence test.

No. i	Grid Number	$v_{in}[\text{mm/s}]$	$ v_{in}^{i+1} - v_{in}^i /v_{in}^i$	$Q_v [(\text{m}^3/\text{s}) \times 10^{-11}]$	$ Q_v^{i+1} - Q_v^i /Q_v^i$	Computing Time
0	51,183	7.3401	/	7.9226	/	3 min 39 s
1	351,336	7.2484	1.249%	7.7683	1.948%	9 min 25 s
2	401,948	7.1848	0.877%	7.6458	1.577%	12 min 41 s
3	1,350,140	7.1614	0.326%	7.6277	0.237%	40 min 35 s
4	1,697,420	7.1643	0.040%	7.6358	0.106%	1 h 26 min 52 s

Besides the mesh independence test, this paper also validates the correctness of the numerical method by performing data validation using references [37,49]. Figure 2a compares the effects of the diameter ratio on the volume flow rate of pure PDF, pure EOF, and the combined EOF and PDF, respectively, within tree-like microchannels with a uniform circular cross-section obtained by the present method with the results in Ref. [37]. Figure 2b presents the EOF velocity profiles of the combined EOF and PDF within a simplified two-dimensional model with a convergence angle of 120° under different driven voltages when $Re = 0.1$ obtained by the present method and from Ref. [49]. Figure 2 shows that the results achieved by the present method are in line with those from the literature, demonstrating the viability of the current numerical method.

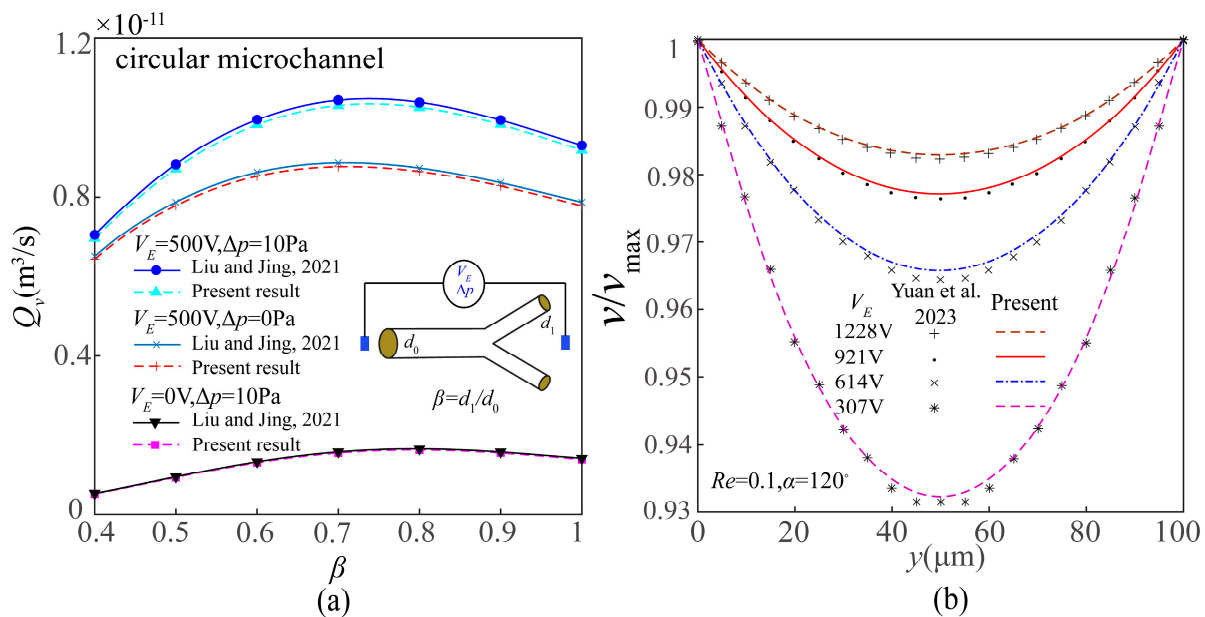


Figure 2. (a) Comparisons of the effects of diameter ratio on flowrate of the combined EOF and PDF within a tree-like microchannel with uniform circular cross-section using present numerical method with the results from Ref. [37] and (b) comparisons of EOF velocity profile within a two-dimensional model using present numerical method with the results from Ref. [49].

4. Results and Discussions

4.1. Impact of Branch Convergence Ratio on the Flow rate within FTCMC

Although previous research [37,50,51] has shown that the combined EOF and PDF for Newtonian fluid satisfies the flow-rate superposition within a single straight microchannel, that is, the sum of the flow rates of pure PDF and pure EOF is equal to the flow rate of the combination of PDF and EOF, the flow-rate superposition within an FTCMC still needs to be validated. Therefore, we first test the flow-rate superposition of the combined PDF and EOF within an FTCMC with $m = 1$ and $m = 2$ when $\kappa = 0.9$, $\lambda = 1$, and $N = 2$ under the different branch convergence ratios, as the results demonstrate in Figure 3. Figure 3 indicates that the sum of the flow rates of the pure PDF and pure EOF is equal to the flow rate of the combined PDF and EOF within the FTCMC. This result indicates that the combined PDF and EOF in FTCMC still satisfies the flow rate superposition. By calculating the inlet Reynolds number in our simulations, we find that the maximum inlet Reynolds number is approximately 50 in our study, which explains why the linear superposition holds true for the FTCMC because the nonlinear effect is negligible at such a low Reynolds number.

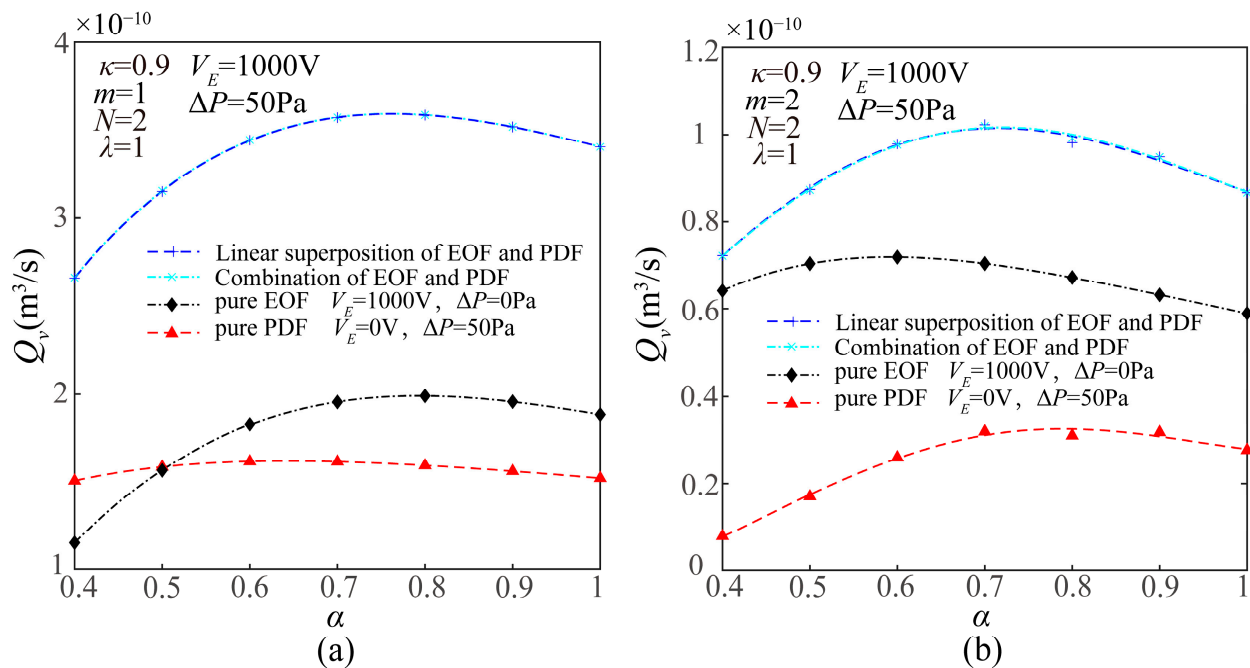


Figure 3. Effects of branch width convergence ratio on the flow rates of pure PDF, pure EOF, and the combined EOF and PDF within the FTCMC with (a) $m = 1$ and (b) $m = 2$ when $\lambda = 1$, $N = 2$, $H = 150 \mu\text{m}$.

In addition, the results in Figure 3 show that the flow rates of pure PDF, pure EOF, and the combined PDF and EOF initially increase and subsequently decrease with the growing branch width convergence ratio, and the values of the branch width convergence ratio to maximize the flow rate are different for three different flow conditions.

By further adjusting the level convergence ratio, Figure 4 displays the influence of the branch width convergence ratio on the flow rate of the combination of EOF and PDF within FTCMCs with different levels of convergence ratios when $m = 1$ or $m = 2$. It can be found that the non-monotonic variation of the flow rate of the combined PDF and EOF within the FTCMC with the growing branch convergence ratio is robust for different values of the fixed-level convergence ratio. It is evident that the FTCMC for each level convergence ratio has an optimal branch convergence ratio α_{opt} corresponding to the maximum flow rate under the fixed external energy input. The reason for these results is that the width of the parent branch declines, while the width of the son branch grows with the increasing branch convergence ratio α under the fixed channel volume, as seen in the geometric dimensions

derived from Equation (1). The reciprocal alteration of the cross-sectional dimensions between the parent branch and son branch results in the emergence of α_{opt} of the FTCMC to maximize the flow rate. The existence of this optimal width convergence ratio is similar to Murray's law, which gives the optimal diameter ratio of the vascular or respiratory network of animals to minimize fluid resistance [45].

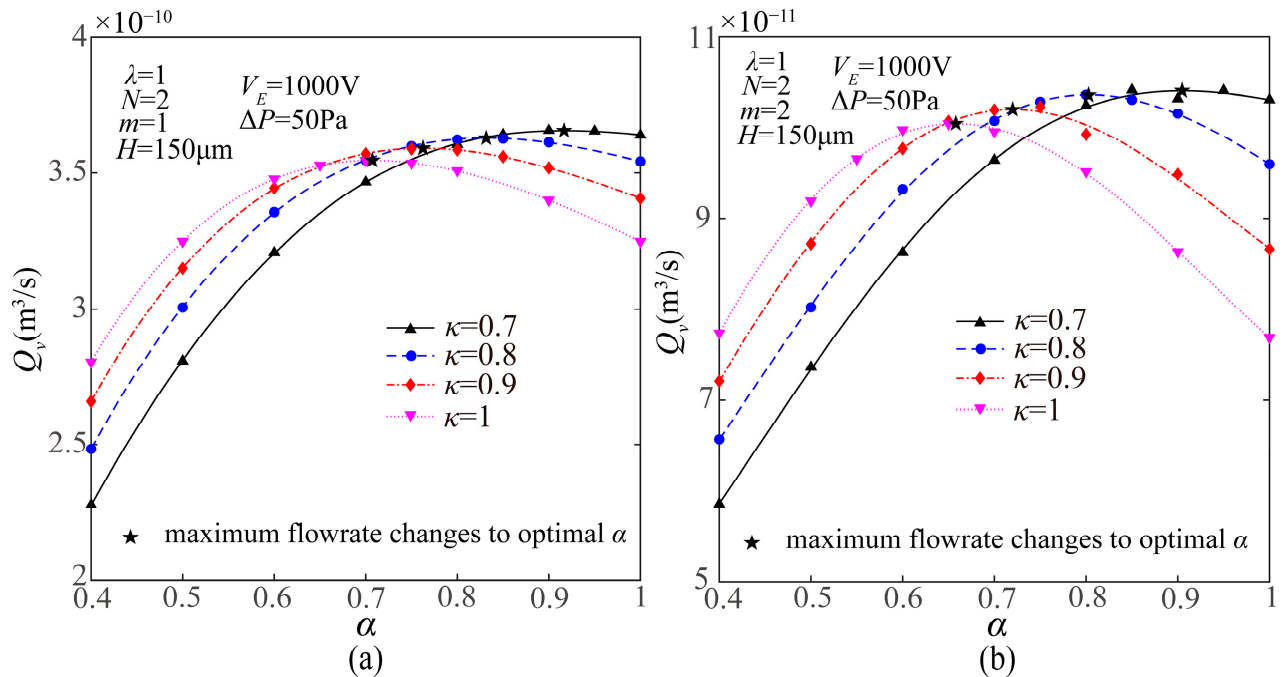


Figure 4. Effects of branch convergence ratio α on the flow rate of the combined EOF and PDF within the FTCMC at different level convergence ratios when $\lambda = 1$, $N = 2$, $H = 150\ \mu\text{m}$, and (a) $m = 1$ and (b) $m = 2$.

From Figure 4, it can further be found that the optimal branch convergence ratio is related to the level convergence ratio. Next, we will investigate the impacts of different parameters on the optimal branch width convergence ratio of FTCMC.

4.2. Impact of Ratio of Voltage Difference and Pressure Difference on α_{opt}

Here, we first investigate the influence of $V_E/\Delta P$ on α_{opt} of the FTCMC at different level convergence ratios κ , as the results illustrated in Figure 5. Figure 5 illustrates that α_{opt} of the FTCMC monotonically decreases with the growing $V_E/\Delta P$. The explanation for this phenomenon is as follows. When $V_E/\Delta P$ remains at a sufficiently low level, the flow rate of the combined flow is dominated by the PDF component; thus, α_{opt} of FTCMC comes close to the value to achieve a maximum pure PDF flow rate. In contrast, when $V_E/\Delta P$ is large enough, the flow rate of the combined PDF and EOF is dominated by the EOF component, and α_{opt} of FTCMC comes close to the value to achieve a maximum pure EOF flow rate. Based on our previous study on the optimal diameter ratio of the fractal tree-like microchannel network with a uniform circular cross-section for maximizing the flow rate of the combined EOF and PDF, the optimal diameter ratio monotonously declines from $N^{-1/3}$ for the pure PDF to $N^{-1/2}$ for the pure EOF with the growing $V_E/\Delta P$ [37]. Similarly, there exists a similar variation trend for the optimal branch convergence ratio α_{opt} of the FTCMC.

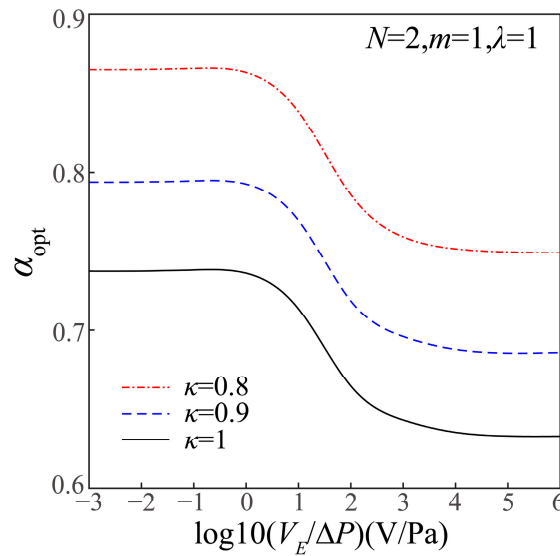


Figure 5. Effect of $V_E/\Delta P$ on α_{opt} of the FTCCM.

4.3. Impacts of Length Ratio, Branching Number, and Branching Level on α_{opt}

Figure 6 shows the influence of the length ratio λ on α_{opt} of the FTCCM under different $V_E/\Delta P$. From Figure 6, it is evident that α_{opt} of the FTCCM increases for the pure PDF but decreases for the pure EOF with the growing length ratio. Further, α_{opt} of the FTCCM for the combined EOF and PDF first decreases and then increases with the increasing length ratio when the $V_E/\Delta P$ gradually increases. This is because the proportion of the EOF component in the total flow rate of combined EOF and PDF within the FTCCM rises when $V_E/\Delta P$ increases, and correspondingly, the impact of λ on α_{opt} is similar to the variation of α_{opt} on the length ratio for pure EOF. In contrast, the variation of α_{opt} of the FTCCM for the combined flow is similar to the variation of α_{opt} on the length ratio for pure PDF when $V_E/\Delta P$ is small because pure PDF dominates the flow rate of the combined EOF and PDF.

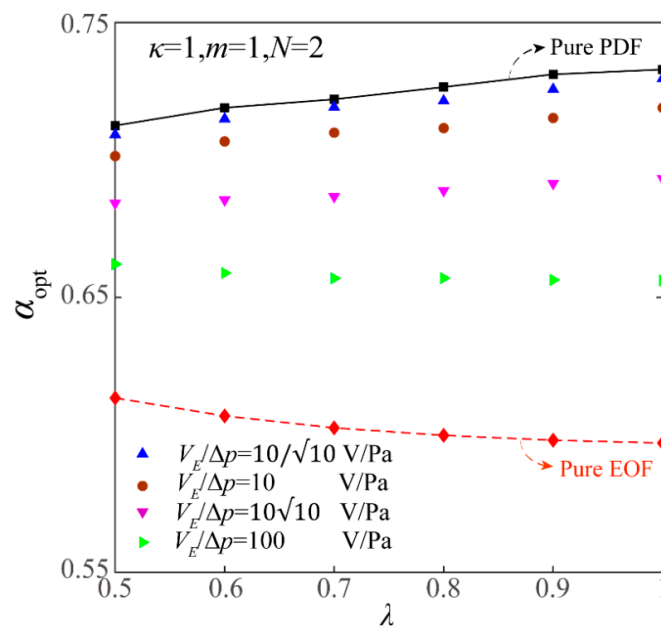


Figure 6. Effect of λ on α_{opt} of the FTCCM under different $V_E/\Delta P$.

Figure 7 shows the effect of the branching number N on α_{opt} of the FTCCM under different $V_E/\Delta P$. Figure 7 indicates that the optimal branch width convergence α_{opt} of the FTCCM for pure EOF, pure PDF, and the combination of EOF and PDF all decrease with

the increasing N , and the optimal branch with the convergence ratio α_{opt} of the FTCMC for the combined EOF and PDF will become closer to the variation of α_{opt} on the N for pure EOF with the increasing $V_E/\Delta P$.

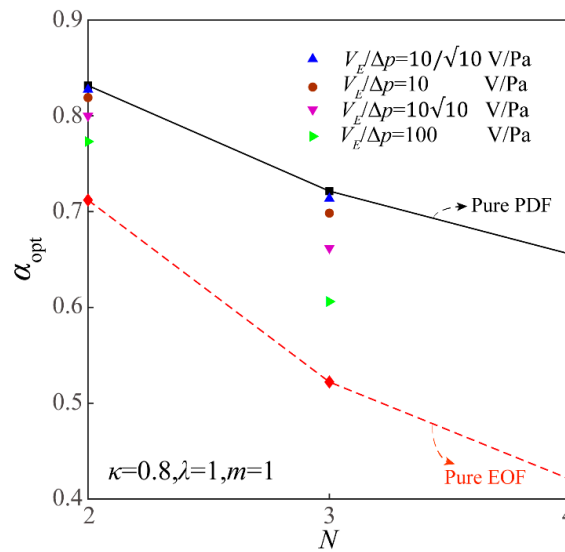


Figure 7. Effect of the branching number on α_{opt} of the FTCMC under different $V_E/\Delta P$.

Further, Figure 8 investigates the effect of the branching level m on α_{opt} of the FTCMC for the combination of EOF and PDF under different $V_E/\Delta P$. Similarly to the effects of the length ratio on the optimal branch convergence ratio α_{opt} , Figure 8 demonstrates that the optimal branch convergence ratio α_{opt} of the FTCMC for pure EOF grows with the increase of the branching level m , while α_{opt} of FTCMC for pure PDF declines. Moreover, the optimal branch convergence ratio α_{opt} of the FTCMC for the combination of EOF and PDF exhibits different variation patterns depending on the ratio of the voltage difference and the pressure difference. The variation of the α_{opt} on the branching level m follows a transition from increasing α_{opt} with growing m for pure PDF to decreasing α_{opt} with growing m for pure EOF due to the proportional variation of the EOF component and the PDF component in the total flow rate of the combination of EOF and PDF.

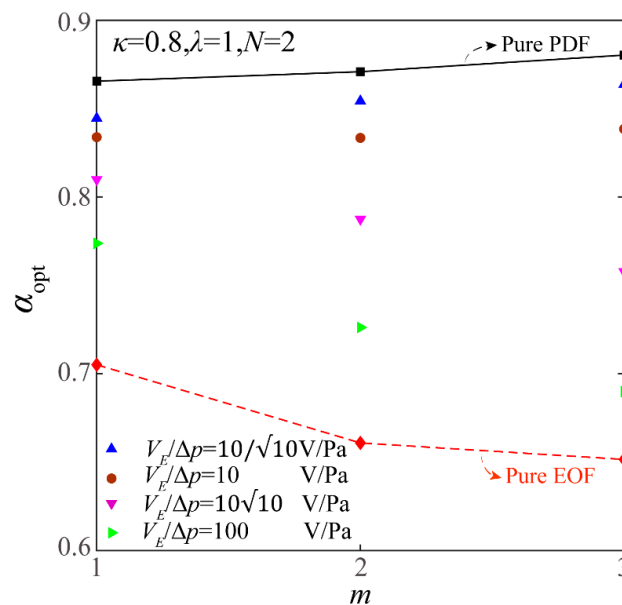


Figure 8. Effect of the branching level on α_{opt} of the FTCMC under different $V_E/\Delta P$.

5. Conclusions

The dimensions of cross-sections play a pivotal role in influencing the flow resistance within microchannels. To analyze the effects of branch cross-sectional convergence on the transport efficiency of the combined EOF and PDF within a fractal tree-like microchannel composed of branches with uniform width convergence ratios and heights, this paper numerically studies the effects of the width convergence ratio on the flow rate of the combined EOF and PDF within the FTCMC under the limitation of the constant total channel volume. Our findings reveal that the flow rate of the combined flow within an FTCMC first increases and then decreases with the growing branch width convergence ratio, indicating the presence of an optimal value α_{opt} to maximize the flow rate of the combined flow. Considering the sensitivity of branch widths on the structural and geometric parameters of the FTCMC such as the level convergence ratio, the branching number, the length ratio, and the branching level of the FTCMC, we examined the effects of these structural and geometric parameters of the FTCMC on the optimal branch width convergence ratio α_{opt} . The effect of the ratio of the voltage difference and the pressure difference on the optimal branch width convergence ratio α_{opt} is also analyzed.

In the parameter setup of the present work, it is found that the optimal branch convergence ratio α_{opt} of the FTCMC monotonically declines with the growing ratio of the voltage difference and the pressure difference and exhibits a transition from the optimal ratio for pure PDF to the optimal ratio for pure EOF. This is due to the predominance of the PDF component influencing the flow rate of the combined flow at large $V_E/\Delta P$, while the EOF component predominantly influences the flow rate of the combined flow at small $V_E/\Delta P$. Furthermore, the optimal branch convergence ratio α_{opt} of the FTCMC shows different variation trends with the level convergence ratio, the branching number, the length ratio, and the branching level of the FTCMC, which is dependent on the ratio of voltage difference and pressure difference.

Although the present findings are highly sensitive to the parameter setup of the FTCMC, they provide a strategy to optimize the transport efficiency of the combined EOF and PDF within a fractal tree-like microchannel with branch convergence, which can inspire potential applications of FTCMC for the cooling and thermal management of microelectronic devices, drug delivery, and screening, as well as catalyst synthesis and separation purification in the chemical industry, etc. [9,52,53], through structural optimization.

Author Contributions: Conceptualization, D.J.; Software, P.Q.; Validation, D.J. and P.Q.; Formal analysis, P.Q. and D.J.; Investigation, P.Q. and D.J.; Data curation, P.Q. and D.J.; Writing—original draft, P.Q.; Writing—review & editing, D.J.; Visualization, P.Q.; Supervision, D.J.; Funding acquisition, D.J. All authors have read and agreed to the published version of the manuscript.

Funding: This research was funded by the National Natural Science Foundation of China with Grant No. 12272236.

Data Availability Statement: The data that support the findings of this study are available from the corresponding author upon reasonable request.

Conflicts of Interest: The authors declare no conflict of interest.

Nomenclature

c	ions concentration
c_{inlet}	inlet concentration
D_c	diffusion coefficient
e	elementary charge
E	applied electric field strength
H	channel height
k_b	Boltzmann constant
l_i	each channel length
m	branching level

n_0	liquid bulk ionic concentration
N	branching number
p	fluid pressure
p_{inlet}	inlet pressure
p_{outlet}	outlet pressure
Q_v	flow rate
Re	Reynolds number
S_i	each channel bottom area
T	absolute temperature
\mathbf{v}	velocity vector
V_i	each channel volume
V	total channel volume
V_E	voltage
w_i	each channel width
z	chemical valence of ions
Greek letters	
α	branch convergence
α_{opt}	optimal branch convergence
β	branch angle
Δp	pressure drop
ε_0	vacuum permittivity
ε_r	relative permittivity of liquid
ζ	zeta potential
κ	level convergence
λ	length ratio
μ	fluid dynamic viscosity
ρ	fluid density
ρ_e	net charge density
φ	applied electric potential
φ_{inlet}	inlet potential
φ_{outlet}	outlet potential
Φ	electrical potential
ψ	EDL electric potential
Abbreviations	
EDL	electrical double layer
EOF	electroosmotic flow
PDF	pressure driven flow
FTCMC	fractal tree-like convergent microchannel

References

- Li, D.Q. *Encyclopedia of Microfluidics and Nanofluidics*; Springer: New York, NY, USA, 2008.
- Lin, B. *Microfluidics: Technologies and Applications*; Springer: Berlin/Heidelberg, Germany, 2011.
- Kandlikar, S.G.; Garimella, S.; Li, D.Q.; Colin, S.; King, M.R. *Heat Transfer and Fluid Flow in Minichannels and Microchannels*; Elsevier: Oxford, UK, 2006.
- Beebe, D.J.; Mensing, G.A.; Walker, G.M. Physics and applications of microfluidics in biology. *Annu. Rev. Biomed. Eng.* **2002**, *4*, 261–286. [[CrossRef](#)] [[PubMed](#)]
- Bojang, A.A.; Wu, H.S. Design, fundamental principles of fabrication and applications of microreactors. *Processes* **2020**, *8*, 891. [[CrossRef](#)]
- Yao, X.; Zhang, Y.; Du, L.; Liu, J.; Yao, J. Review of the applications of microreactors. *Renew. Sustain. Energy Rev.* **2015**, *47*, 519–539. [[CrossRef](#)]
- Shourabi, A.Y.; Kashaninejad, N.; Saidi, M.S. An integrated microfluidic concentration gradient generator for mechanical stimulation and drug delivery. *J. Sci. Adv. Mater. Devices* **2021**, *6*, 280–290. [[CrossRef](#)]
- Bejan, A.; Zane, J.P. Design in Nature. *Mechical Eng.* **2012**, *134*, 42–47. [[CrossRef](#)]
- Xu, P.; Sasmito, A.P.; Yu, B.; Mujumdar, A.S. Transport phenomena and properties in tree-like networks. *Appl. Mech. Rev.* **2016**, *68*, 040802. [[CrossRef](#)]
- Samal, S.K.; Qadeer, M.; Saha, S.K. thermo-hydraulic performance evaluation of radial tree-branching microchannel heat sinks for electronic cooling applications. *Int. J. Therm. Sci.* **2024**, *197*, 108800. [[CrossRef](#)]

11. Chen, Y.; Cheng, P. Heat transfer and pressure drop in fractal tree-like microchannel nets. *Int. J. Heat Mass. Transf.* **2002**, *45*, 2643–2648. [[CrossRef](#)]
12. Ji, X.; Yang, X.; Zhang, Y.; Zhang, Y.; Wei, J. Experimental study of ultralow flow resistance fractal microchannel heat sinks for electronics cooling. *Int. J. Therm. Sci.* **2022**, *179*, 107723. [[CrossRef](#)]
13. Ma, C.; Sun, Y.; Wu, Y.; Zhang, Q.; Wang, Y.; Ding, G. A bio-inspired fractal microchannel heat sink with secondary modified structure and sub-total-sub fluid transmission mode for high heat flux and energy-saving heat dissipation. *Int. J. Heat Mass Transf.* **2023**, *202*, 123717. [[CrossRef](#)]
14. Lovchik, R.D.; Tonna, N.; Bianco, F.; Matteoli, M.; Delamarche, E. A microfluidic device for depositing and addressing two cell populations with intercellular population communication capability. *Biomed. Microdevices* **2010**, *12*, 275–282. [[CrossRef](#)] [[PubMed](#)]
15. Lu, H.; Koo, L.Y.; Wang, W.M.; Lauffenburger, D.A.; Griffith, L.G.; Jensen, K.F. Microfluidic shear devices for quantitative analysis of cell adhesion. *Anal. Chem.* **2004**, *76*, 5257–5264. [[CrossRef](#)] [[PubMed](#)]
16. Senn, S.M.; Poulidakos, D. Laminar mixing, heat transfer and pressure drop in tree-like microchannel nets and their application for thermal management in polymer electrolyte fuel cells. *J. Power Sources* **2004**, *130*, 178–191. [[CrossRef](#)]
17. Kjelstrup, S.; Coppens, M.O.; Pharoah, J.G.; Pfeifer, P. Nature-inspired energy- and material-efficient design of a polymer electrolyte membrane fuel cell. *Energy Fuels* **2010**, *24*, 5097–5108. [[CrossRef](#)]
18. Chakraborty, S. *Microfluidics and Microfabrication*; Springer: Boston, MA, USA, 2010.
19. Karniadakis, G.E.; Beskok, A.; Gad-el-Hak, M. Micro flows: Fundamentals and Simulation. *Appl. Mechanics Rev.* **2002**, *55*, B76. [[CrossRef](#)]
20. Jing, D.; Bhushan, B. The coupling of surface charge and boundary slip at the solid–liquid interface and their combined effect on fluid drag: A review. *J. Colloid Interface Sci.* **2015**, *454*, 152–179. [[CrossRef](#)] [[PubMed](#)]
21. Li, D. *Electrokinetics in Microfluidics*; Academic Press: Oxford, UK, 2004.
22. Chen, Q.; Shyu, S.; Li, W. An overlapped electrical double layer model for aqueous electrolyte lubrication with asymmetric surface electric potentials. *Tribol. Int.* **2020**, *147*, 106283. [[CrossRef](#)]
23. Sasaki, N.; Kitamori, T.; Kim, H.B. AC electroosmotic micromixer for chemical processing in a microchannel. *Lab A Chip* **2006**, *6*, 550–554. [[CrossRef](#)] [[PubMed](#)]
24. Wang, X.; Cheng, C.; Wang, S.; Liu, S. Electroosmotic pumps and their applications in microfluidic systems. *Microfluid. Nanofluidics* **2009**, *6*, 145–162. [[CrossRef](#)]
25. Dutta, P.; Horiuchi, K.; Yin, H.-M. Thermal Characteristics of Mixed Electroosmotic and Pressure-Driven Microflows. *Comput. Math. Appl.* **2006**, *52*, 651–670. [[CrossRef](#)]
26. Babaie, A.; Sadeghi, A.; Saidi, M.H. Combined electroosmotically and pressure driven flow of power-law fluids in a slit microchannel. *J. Non-Newton. Fluid Mech.* **2011**, *166*, 792–798.
27. Ebrahimi, S.; Hasanzadeh-Barforoushi, A.; Nejat, A.; Kowsary, F. Numerical study of mixing and heat transfer in mixed electroosmotic/pressure driven flow through T-shaped microchannels. *Int. J. Heat Mass Transf.* **2014**, *75*, 565–580. [[CrossRef](#)]
28. Mondal, M.; Misra, R.P.; De, S. Combined electroosmotic and pressure driven flow in a microchannel at high zeta potential and overlapping electrical double layer. *Int. J. Therm. Sci.* **2014**, *86*, 48–59. [[CrossRef](#)]
29. Deng, S.; Xiao, T.; Liang, C. Analytical study of unsteady two-layer combined electroosmotic and pressure-driven flow through a cylindrical microchannel with slip-dependent zeta potential. *Chem. Eng. Sci.* **2024**, *283*, 119327. [[CrossRef](#)]
30. Hegde, A.S.; Harikrishnan, A.R. Slip hydrodynamics of combined electroosmotic and pressure driven flows of power law fluids through narrow confinements. *Eur. J. Mech. B/Fluids* **2021**, *89*, 525–550.
31. Feng, Q.; Chen, X.; Wang, X.; Yu, X.; Zeng, X.; Ma, Y.; Wang, Q. Numerical simulation of a three dimensional electroosmotic micromixer with a flexible and controllable Rubik’s cube module. *Int. Commun. Heat Mass Transf.* **2021**, *127*, 105482. [[CrossRef](#)]
32. An, S.; Tian, K.; Ding, Z.; Jian, Y. Electroosmotic and pressure-driven slip flow of fractional viscoelastic fluids in microchannels. *Appl. Math. Comput.* **2022**, *425*, 127073. [[CrossRef](#)]
33. Alshammari, F.S.; Akyildiz, F.T. Pseudo spectral solution of extended Graetz problem for combined pressure-driven and electroosmotic flow in a triangular micro-duct. *Comput. Math. Appl.* **2020**, *80*, 990–1008. [[CrossRef](#)]
34. Barrot, C.; Colin, S.P. Electroosmotic flow in tree-shaped microchannel networks. In Proceedings of the 6th International Conference on Nanochannels, Microchannels, and Minichannels, Darmstadt, Germany, 23–25 June 2008; Volume 48345, pp. 419–426.
35. Barrot, C.; Colin, S.P. Design of tree-shaped microchannel networks submitted to simultaneous pressure driven and electroosmotic flows. In Proceedings of the 10th International Conference on Nanochannels, Microchannels, and Minichannels, Rio Grande, PR, USA, 8–12 July 2012; Volume 44793, pp. 113–121.
36. Jing, D.; Yi, S. Electroosmotic flow in tree-like branching microchannel network. *Fractals* **2019**, *27*, 1950095. [[CrossRef](#)]
37. Liu, F.; Jing, D. Combined electroosmotic and pressure driven flow in tree-like microchannel network. *Fractals* **2021**, *29*, 2150110. [[CrossRef](#)]
38. Zhang, J.; Shu, S.; Guan, X.; Yang, N. Lattice Boltzmann simulation of drop splitting in a fractal tree-like microchannel. *Chem. Eng. Sci.* **2022**, *252*, 117277. [[CrossRef](#)]
39. Khan, M.A.; Suhaib, M.; Ansari, M.A. Investigations on fluid flow and mixing in fractal tree like biomimetic microchannel based on Murray’s law. *Chem. Eng. Process. Process Intensif.* **2023**, *194*, 109564. [[CrossRef](#)]
40. Zhu, R.; Jing, D. Numerical study on the discharging performance of a latent heat thermal energy storage system with fractal tree-shaped convergent fins. *Renew. Energy* **2024**, *221*, 119726. [[CrossRef](#)]

41. Zhu, R.; Jing, D. Numerical study on thermal and melting performances of a horizontal latent heat storage unit with branched tree-like convergent fins. *J. Energy Storage* **2023**, *62*, 106889. [[CrossRef](#)]
42. Qi, P.; Jing, D. Experimental and numerical study on the hydrothermal performances of a mirror Y-shaped convergent mini-channel heat sink. *Case Stud. Therm. Eng.* **2024**, *53*, 103966. [[CrossRef](#)]
43. Liu, F.; Zhu, R.; Jing, D. Hydraulic and thermal performances of tree-like convergent microchannel heat sinks. *Fractals* **2022**, *30*, 2250096. [[CrossRef](#)]
44. Chakraborty, S.; Mondal, N.; Bakli, C. Passive building cooling using tree-shaped converging microchannel nets. In *AIP Conference Proceedings, Proceedings of the 2nd International Conference on Recent Advances in Fluid and Thermal Sciences 2020 (iCRAFT2020), Dubai, United Arab Emirates, 19–21 March 2021*; AIP Publishing: Melville, NY, USA, 2023; Volume 2584, p. 050001.
45. Murray, C.D. The physiological principle of minimum work: I. The vascular system and the cost of blood volume. *Proc. Natl. Acad. Sci. USA* **1926**, *12*, 207–214. [[CrossRef](#)]
46. Miguel, A.F. Fluid flow in a porous tree-shaped network: Optimal design and extension of Hess–Murray’s law. *Phys. A Stat. Mech. Its Appl.* **2015**, *423*, 61–71.
47. Patankar, N.A.; Hu, H.H. Numerical simulation of electroosmotic flow. *Anal. Chem.* **1998**, *70*, 1870–1881. [[CrossRef](#)] [[PubMed](#)]
48. Kang, Y.; Yang, C.; Huang, X. Electroosmotic flow in a capillary annulus with high zeta potentials. *J. Colloid Interface Sci.* **2002**, *253*, 285–294. [[CrossRef](#)] [[PubMed](#)]
49. Yuan, S.; Zhou, M.; Liu, X.; Jiang, B. Effect of pressure-driven flow on electroosmotic flow and electrokinetic mass transport in microchannels. *Int. J. Heat Mass Transf.* **2023**, *206*, 123925. [[CrossRef](#)]
50. Ng, C.O.; Qi, C. Electroosmotic flow of a power-law fluid in a non-uniform microchannel. *J. Non-Newton. Fluid Mech.* **2014**, *208*, 118–125.
51. Dutta, P.; Beskok, A. Analytical solution of combined electroosmotic/pressure driven flows in two-dimensional straight channels: Finite Debye layer effects. *Anal. Chem.* **2001**, *73*, 1979–1986. [[CrossRef](#)] [[PubMed](#)]
52. Miguel, A.F.; Rocha, L.A. *Tree-Shaped Fluid Flow and Heat Transfer*; Springer International Publishing: Cham, Switzerland, 2018.
53. Yu, H.; Zhang, J.; Zhang, S.; Han, Z. Bionic Struct. Mater. Inspired By Plant Leaves: A comprehensive review for innovative problem-solving. *Prog. Mater. Sci.* **2023**, *139*, 101181. [[CrossRef](#)]

Disclaimer/Publisher’s Note: The statements, opinions and data contained in all publications are solely those of the individual author(s) and contributor(s) and not of MDPI and/or the editor(s). MDPI and/or the editor(s) disclaim responsibility for any injury to people or property resulting from any ideas, methods, instructions or products referred to in the content.